Towards adiabatic quantum computing using compressed quantum circuits

Conor Mc Keever* and Michael Lubasch
Quantinuum, Partnership House, Carlisle Place, London SW1P 1BX, United Kingdom
(Dated: November 9, 2023)

We describe tensor network algorithms to optimize quantum circuits for adiabatic quantum computing. To suppress diabatic transitions, we include counterdiabatic driving in the optimization and utilize variational matrix product operators to represent adiabatic gauge potentials. Traditionally, Trotter product formulas are used to turn adiabatic time evolution into quantum circuits and the addition of counterdiabatic driving increases the circuit depth per time step. Instead, we classically optimize a parameterized quantum circuit of fixed depth to simultaneously capture adiabatic time evolution together with counterdiabatic driving over many time steps. The methods are applied to the ground state preparation of quantum Ising chains of sizes $N = 7 - 31$ with transverse and longitudinal fields. We show that the classically optimized circuits can significantly outperform Trotter product formulas. Furthermore, we discuss how the approach can be used for combinatorial optimization.

I. INTRODUCTION

To make use of current quantum computing technologies, adiabatic time evolution [1–4] is a promising concept that underpins, for example, the computations of the famous D-Wave device [5] and motivates the popular quantum approximate optimization algorithm [6]. In the adiabatic approach, the quantum device prepares a trivial ground state and then realizes time evolution with a specific, time-dependent Hamiltonian, whose initial ground state is the trivial one and whose final ground state encodes the desired quantum computational result. The procedure is successful if the evolution occurs sufficiently slowly and the total evolution time scales $\propto 1/\Delta^2$ [7] where Δ is the minimum energy difference between the ground and the first excited state during the evolution. On digital quantum computers, time evolution can be readily realized using Trotter product formulas [8], but long evolution times can lead to deep circuits. One powerful tool to reduce the adiabatic evolution time is the so-called counterdiabatic driving [9–11], in which additional terms are included in the Hamiltonian to suppress unwanted transitions during the time evolution. These additional Hamiltonian terms, however, lead to deeper Trotter circuits per time step on a gate-based quantum device. Therefore, adiabatic time evolution over many time steps, with or without counterdiabatic driving, can still be a challenge for current digital quantum computers.

In this article, we propose to classically optimize parameterized quantum circuits (PQCs) [12–14] to represent adiabatic time evolution with counterdiabatic driving. We extend the tensor network [15–17] toolbox for quantum circuit optimization of Hamiltonian simulation [18–20] to tackle adiabatic quantum computing. Figure 1 gives an overview of our approach. The PQC compression of adiabatic time evolution for each chunk in Fig. 1 (e) can be performed such as to exhaust the capabilities of classical computing. Then appending all PQCs, as depicted in Fig. 1 (e), can create a quantum state that is hard to simulate for classical computers but efficient to realize on a quantum computer and, therefore, has the potential to provide a quantum advantage. We numerically demonstrate that, compared with Trotter circuits, the classically optimized PQCs lead to significantly better ground state fidelities and energy accuracies in the context of quantum Ising chains. An important ingredient in counterdiabatic driving is the adiabatic gauge potential [21] and we study the suitability of a variational matrix product operator (MPO) [22, 23] ansatz for it. The MPO ansatz naturally fits within our tensor network approach and we also show that it can have advantages over the popular nested commutator ansatz [24]. While all numerical benchmarks are carried out on particular, one-dimensional quantum many-body systems, it is straightforward to generalize the algorithms to solve higher-dimensional problems as well as combinatorial optimization.

The article has the following structure. Section II contains the description of the numerical methods, including the variational optimization of the MPO gauge potential in Sec. II A and the PQCs for the adiabatic evolution in Sec. II B. In Sec. III, we present the results of this study, i.e. the comparison between the nested-commutator and the MPO gauge potentials in Sec. III A as well as the comparison between the Trotter and the classically optimized circuits in Sec. III B. We discuss how to adapt the circuit optimization procedures for other problems, such as combinatorial optimization, in Sec. IV. Technical details are provided in the Appendixes.

II. METHODS

We consider the protocol that is explained in Fig. 1 and which is based on time evolution according to a

* conor.mckeever@quantinuum.com

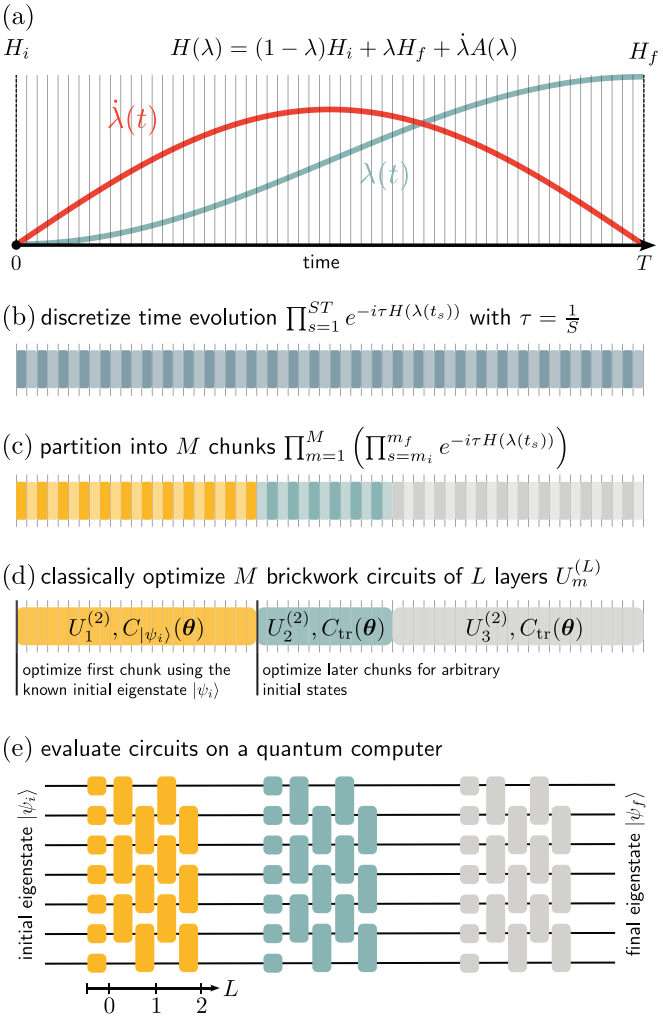

FIG. 1. The proposed optimization procedure. (a) We consider adiabatic evolution for total time T according to a time-dependent Hamiltonian $H(\lambda(t))$ with gauge potential $A(\lambda(t))$ [21] where $\lambda(0) = 0$ and $\lambda(T) = 1$. (b) The total evolution over time T is cut into ST slices of shorter evolutions over small time steps $\tau = 1/S$. For the evolution of each slice, we assume $\lambda(t) = \lambda(t_s)$ where t_s is the midpoint of slice s, so that during every slice evolution the Hamiltonian is time-independent. (c) We split the total evolution time T into M chunks and assign the slices to their corresponding chunks. (d) For each chunk, we optimize a PQC with variational parameters $\boldsymbol{\theta}$ to represent the corresponding evolution. The PQC optimization proceeds one slice after another as in [20] for all chunks except for the first one, for which we minimize a cost function $C_{|\psi_i\rangle}(\boldsymbol{\theta})$ that takes into account the initial state $|\psi_i\rangle$. (e) After the classical optimization, the resulting circuits can be run on a gate-based quantum device and realize the adiabatic quantum computation.

Schrödinger equation

$$\mathrm{i}\partial_t|\psi\rangle = H(\lambda(t))|\psi\rangle, \tag{1}$$

where $\hbar = 1$ in our system of units and the time-dependent Hamiltonian $H(\lambda(t))$ has the form shown in Fig. 1 (a). At the beginning, $t = 0$, $H(\lambda(0)) = H(0)$ is equivalent to the initial Hamiltonian, H_i, whose ground state is the initial eigenstate $|\psi_i\rangle$. At the end, $t = T$, $H(\lambda(T)) = H(1)$ is equivalent to the final Hamiltonian, H_f, whose ground state is the final eigenstate $|\psi_f\rangle$. During the evolution, $H(\lambda)$ is a linear combination of H_i and H_f and, additionally, contains a contribution from the adiabatic gauge potential A [21], see Appendix A.

A. Variational MPOs for the adiabatic gauge potential

We obtain the gauge potential A using a variational procedure [21] based on an MPO ansatz that we numerically optimize to minimize a certain cost function, see Appendix B. The MPO ansatz is characterized by the MPO bond dimension χ that determines the expressive power and computational cost related to the ansatz [22, 23]. For the optimization, it is useful to write the variational gauge potential operator $\tilde{A}$ as a state $|\tilde{A}\rangle$ (by making use of the well-known Choi-Jamiołkowski isomorphism). Then the cost function can be conveniently expressed in terms of a system of linear equations

$$(\mathcal{H}\otimes\mathbb{1} - \mathbb{1}\otimes\mathcal{H}^T)|\tilde{A}\rangle = -\mathrm{i}|\partial_\lambda\mathcal{H}\rangle, \tag{2}$$

cf. Eq. (B16), where $\mathbb{1}$ denotes the identity operator, $\mathcal{H}$ is $H(\lambda)$ without the gauge potential, i.e. in our case $\mathcal{H} = (1-\lambda)H_i + \lambda H_f$, and $(\cdot)^T$ is the transpose of $(\cdot)$. The matrix $(\mathcal{H}\otimes\mathbb{1} - \mathbb{1}\otimes\mathcal{H}^T)$ is rank-deficient and so we add a small regularization parameter η to its diagonal. Then the variational optimization proceeds using tensor network algorithms for linear equations [25, 26].

B. Classical optimization of counterdiabatic dynamics

For the circuit optimization we use an iterative procedure which generalizes [20] to time-dependent Hamiltonians. The procedure is illustrated in Fig. 1 (b-d). At each time slice $s = 1, 2, \ldots, ST$, the short-time evolution operator is approximated using a first-order Taylor approximation

$$e^{-\mathrm{i}\tau(\mathcal{H}_s + \dot{\lambda}_s\tilde{A}_s)} = \mathbb{1} - \mathrm{i}\tau\mathcal{H}_s - \mathrm{i}\tau\dot{\lambda}_s\tilde{A}_s + O(\tau^2). \tag{3}$$

Here $\mathcal{H}_s$, $\dot{\lambda}_s$ and $\tilde{A}_s$ are equivalent to $\mathcal{H}$, $\dot{\lambda}$ and $\tilde{A}$ evaluated at time slice s, respectively. The operator $W_s = \mathbb{1} - \mathrm{i}\tau\mathcal{H}_s + O(\tau^2)$ can be represented efficiently as an MPO using the W^I or W^{II} method from [27] or, for higher orders of τ, using the approach of [28]. The operator $\tilde{A}_s$ is an MPO representation of the adiabatic gauge potential that is calculated using the variational method of Sec. II A.

At slice q of chunk $m \in \{1, 2, \ldots, M\}$ of the iterative circuit optimization procedure we minimize the cost

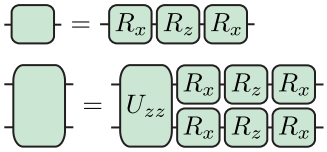

FIG. 2. Parameterized quantum gates $R_x(\theta) = \exp(-\mathrm{i}\theta X/2)$, $R_z(\theta) = \exp(-\mathrm{i}\theta Z/2)$ and $U_{zz}(\theta) = \exp(-\mathrm{i}\theta Z\otimes Z/2)$, where θ denotes the variational parameter, for the ansatz in Fig. 1 (e).

function $C^{(q)}(\boldsymbol{\theta})$ over the corresponding L-layer PQC $U(\boldsymbol{\theta}) = U_m^{(L)}$ where

$$C^{(q)}(\boldsymbol{\theta}) = -\,\mathrm{Re}\{\mathrm{tr}[U^\dagger(\boldsymbol{\theta})(W_q - \mathrm{i}\tau\dot{\lambda}_q\tilde{A}_q)U(\boldsymbol{\theta}_{q-1})\rho]\}, \quad (4)$$

where Re denotes the real part, $\mathrm{tr}[(\cdot)]$ the trace of $(\cdot)$, $(\cdot)^\dagger$ adjoint of $(\cdot)$, and $U(\boldsymbol{\theta}_0) = \mathbb{1}$. Knowledge of the initial state can be incorporated into the cost function using the operator ρ. For example, if an efficient MPS representation of the initial state $|\psi_i\rangle$ is known, we set $\rho = |\psi_i\rangle\langle\psi_i|$ and we denote the associated cost function as $C_{|\psi_i\rangle}(\boldsymbol{\theta})$. In the opposite limit, where we have no knowledge of the initial state, the operator ρ is set to the identity $\rho = \mathbb{1}$ and we denote the associated cost function as $C_{\mathrm{tr}}(\boldsymbol{\theta})$. Furthermore, any operator ρ with an efficient MPO representation can be used such as, e.g., a low-bond-dimension approximation to a thermal state. In this article we consider only the two limiting cases of $\rho = \mathbb{1}$ and $\rho = |\psi_i\rangle\langle\psi_i|$.

The result of the classical circuit optimization is a set of circuits $U_m^{(L)}(\boldsymbol{\theta})$ for $m \in \{1, 2, \ldots, M\}$ which can be evaluated on a quantum computer as shown in Fig. 1 (e).

III. RESULTS

In the following, we consider the one-dimensional nearest-neighbour quantum Ising Hamiltonian

$$H_{\mathrm{Ising}} = \sum_{k=1}^{N-1} J_k Z_k Z_{k+1} + \sum_{k=1}^{N} g_k X_k + \sum_{k=1}^{N} h_k Z_k. \quad (5)$$

where J_k, g_k and h_k are parameters of the Hamiltonian at site k and X (Z) is the Pauli X (Z) matrix.

In Sec. III B, we optimize PQCs $U(\boldsymbol{\theta})$ which have a brickwork structure as illustrated in Fig. 1 (e). Each of the M chunks of the brickwork circuits consists of an initial layer of single-qubit blocks followed by L layers of two-qubit blocks arranged in a brickwork pattern. The substructure of each block is shown in Fig. 2.

A. Comparison of variational MPO gauge potential to the nested commutator approach

The nested commutator (NC) method [24] approximates the adiabatic gauge potential in terms of a series of nested commutators of $\mathcal{H}$ and $\partial_\lambda\mathcal{H}$. The order l of the NC approximation corresponds to the number of nested commutators retained in the series. To facilitate a comparison with the NC method [24] we consider an $N = 14$ qubit quantum Ising Hamiltonian Eq. (5) at one point along the adiabatic path, such that $J_k = 1.0$, and $h_k = g_k = 0.3\lambda$ for all qubit indices $k = 1, 2, \ldots, N$. The resulting Hamiltonian is

$$\mathcal{H}(\lambda) = \sum_{k=1}^{13} Z_k Z_{k+1} + 0.3\lambda \sum_{k=1}^{14} (X_k + Z_k)\,. \quad (6)$$

To assess the performance of the variational MPO gauge potential $\tilde{A}$, we compute the values of the normalized cost, defined as

$$\mathrm{tr}\left[G^\dagger(\tilde{A})G(\tilde{A})\right] / \mathrm{tr}\left[\partial_\lambda\mathcal{H}^2\right], \quad (7)$$

and the normalized error

$$\left[G(\tilde{A}), \mathcal{H}\right] / \mathrm{tr}\left[\partial_\lambda\mathcal{H}^2\right] \quad (8)$$

where $[O_1, O_2]$ denotes the commutator of O_1 and O_2, and we refer the reader to Eq. (B1) in Appendix B for a definition of the operator G.

Results for the normalized cost and normalized error, both of which we seek to minimize during the variational optimization, are illustrated in Fig. 3. We observe that the normalized cost in Fig. 3 (a) decreases with increasing variational MPO bond dimension χ and decreasing regularization strength η^2.

For the normalized error in Fig. 3 (b) we observe that, while the error decreases with increasing bond dimension χ, there is an optimal regularization parameter η^2 which minimizes the error for each χ. Additionally, we find that the variationally optimized gauge potentials outperform the nested commutator gauge potential of order $l = 6$ in terms of the normalized error.

Figure 4 shows the maximum bond dimension of the nested commutator gauge potential when represented as an MPO. We use two different techniques to construct these MPOs as described in the caption of Fig. 4. When considered alongside the results of Fig. 3, we observe that the variationally optimized MPO gauge potentials outperform those constructed using the nested commutator approach while also having a much smaller maximum bond dimension.

B. Circuits for counterdiabatic spectral gap traversal

In this section we consider an instance of quantum Ising Hamiltonian Eq. (5) with uniform parameters $J_k = J$, $g_k = g$ and $h_k = h$ for all qubit indices $k = 1, 2, \ldots, N$; we denote this Hamiltonian $H_{\mathrm{Ising}}(J, g, h)$. We consider an adiabatic path that starts with an initial Hamiltonian $H_i = H_{\mathrm{Ising}}(0, g^*, 0)$ and ends with a final Hamiltonian

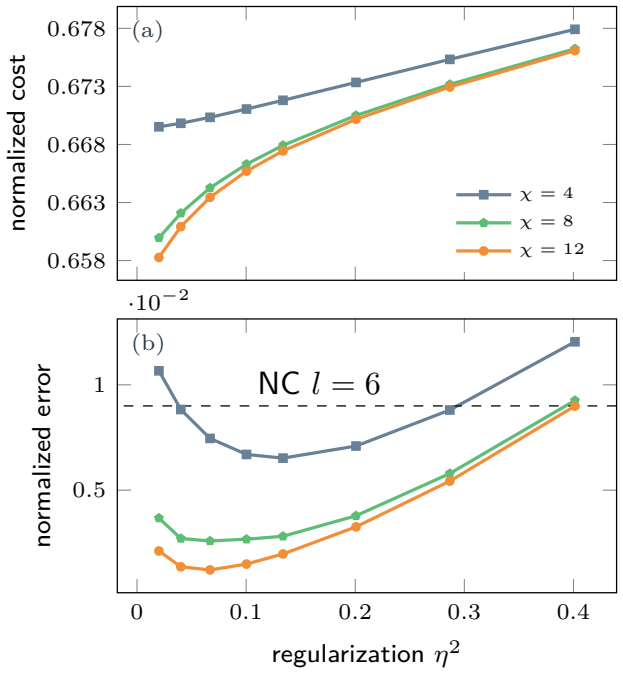

FIG. 3. (a) Normalized cost of Eq. (7) and (b) normalized error of Eq. (8) as a function of the strength of regularization used in the variational MPO method for different bond dimensions. The dashed horizontal line indicates the error achieved by the nested commutator (NC) method of order $l = 6$ as reported in [24].

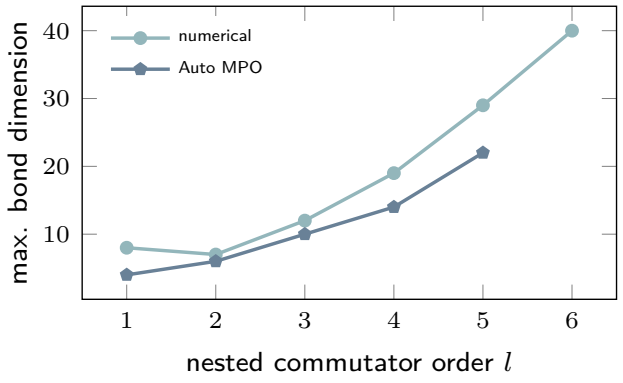

FIG. 4. The maximum bond dimension of the nested-commutator (NC) gauge potential of order l for the $N = 14$ qubit Hamiltonian $\mathcal{H}(\lambda)$ defined in Sec. III B. For each NC order l the prefactors α_k for $k = 1, 2, \ldots, l$ of the NCs are calculated numerically. To construct $\tilde{A}_l$ we use numerical multiplication and addition of MPOs representing $\mathcal{H}$ and $\partial_\lambda \mathcal{H}$ to evaluate and sum over the NCs. As an alternative method, we simplify the nested commutators algebraically using QuantumAlgebra.jl [29] into sums of Pauli strings and construct $\tilde{A}_l$ using the Auto MPO method [30] included in the ITensors.jl library [31].

$H_f = H_{\text{Ising}}(1, g^*, 1)$. The resulting adiabatic Hamiltonian that interpolates between H_i and H_f is therefore $\mathcal{H}(\lambda) = (1-\lambda)H_i + \lambda H_f$, where we choose the path

$$\lambda(t) = \sin\left(\frac{\pi}{2}\sin\left(\frac{\pi t}{2T}\right)\right), \tag{9}$$

such that the rate of change of the path $\dot{\lambda}(t)$ at its beginning and end are zero, so as to switch off the gauge potential at these points. For the chosen parameters, the ground state of $\mathcal{H}$ starts in a paramagnetic phase and ends in an antiferromagnetic phase, crossing the transition between these phases at approximately $\lambda = 0.5$.

The energy difference between the ground and first excited state of $\mathcal{H}(\lambda)$, i.e. the spectral gap, is plotted as a function of λ for system sizes $N \in \{7, 15, 23, 31\}$ in Fig. 5 (a). We observe that the minimum spectral gap Δ decreases as the number of qubits increases.

To proceed, we calculate the adiabatic gauge potentials for system sizes $N \in \{7, 15, 23, 31\}$, variational MPO bond dimensions $\chi \in \{4, 8\}$ and total evolution times $T \in \{0.1, 0.2, 0.3\}$ using the method of Sec. II A. More precisely, we discretize the total times T into ST slices where, in all cases $S = 120$, and calculate the adiabatic gauge potentials $\tilde{A}_s^{(\chi)}$ for each slice.

Since $\dot{\lambda}(t=0) = \dot{\lambda}(t=T) = 0$, the counterdiabatic Hamiltonian $H(\lambda) = \mathcal{H}(\lambda) + \dot{\lambda}\tilde{A}(\lambda)$ still starts with H_i and ends at H_f but differs from $\mathcal{H}(\lambda)$ for $0 < \lambda < 1$. The spectral gap of $H(\lambda)$ as a function of λ for $N = 23$, $\chi = 4$ and $T = 0.3$ is illustrated in Fig. 5 (b), where we observe that the effect of introducing the gauge potential is to increase the spectral gap as compared to $\mathcal{H}(\lambda)$ alone. Additionally we observe in Fig. 5 (c) that the maximum entanglement entropy of the ground state of $H(\lambda)$ along the adiabatic path is increased compared to that of $\mathcal{H}(\lambda)$. Here, the measure of entanglement entropy used is the von-Neumann entropy $S_{\text{VN}} = -\sum_j \xi_j \ln \xi_j$ where ξ_j are the Schmidt coefficients resulting from the bipartition of the ground state MPS at the center of the chain as described in the caption of Fig. 5.

Given the choice of interpolating Hamiltonian, the initial eigenstate, i.e. the ground state of $H(\lambda = 0) = H_i$, corresponds to the product state $|\psi_i\rangle = |-\rangle^{\otimes N}$ and can easily be incorporated into the cost function $C_{|\psi_i\rangle}(\boldsymbol{\theta})$ for the first chunk of the circuit optimization procedure. We optimize brickwork circuits of $M = 2$ chunks and $L = 4$ layers using the method of Sec. II B. After completing all circuit optimizations we are left with a pair of circuits $U_m^{(4)}$ for $m \in \{1, 2\}$ for each parameter set $\{T, \chi, N\}$.

To compare the performance of the counterdiabatic classically optimized circuits to more traditional techniques we also construct circuits using a second-order Trotterization of the standard adiabatic path defined by $\mathcal{H}(\lambda)$. Importantly, we use $R = 8$ Trotter layers such that these circuits contain the same number of two-qubit gates as the classically optimized counterdiabatic circuits of $R = M \times L = 8$ layers. To approximate the adiabatic time dynamics as a Trotter circuit

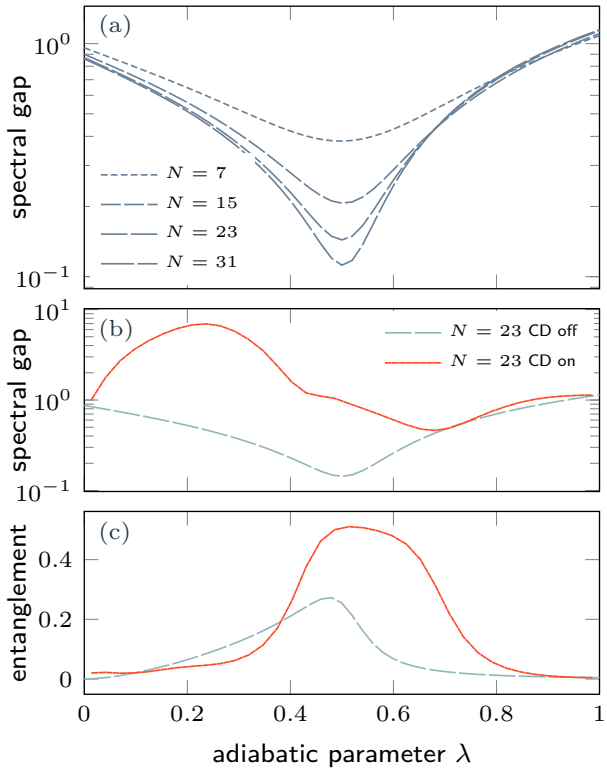

FIG. 5. (a) The spectral gap of the one-dimensional adiabatic Hamiltonian $\mathcal{H}(\lambda) = (1-\lambda)H_i + \lambda H_f$ as a function of the adiabatic parameter λ for a range of qubit counts $N \in \{7, 15, 23, 31\}$ where $H_i = H_{\text{Ising}}(0, g^*, 0)$, $H_f = H_{\text{Ising}}(1, g^*, 1)$ and $H_{\text{Ising}}(J, g, h)$ is the antiferromagnetic Ising Hamiltonian defined in Sec. III B. For each system size $N \in \{7, 15, 23, 31\}$ the strengths of the corresponding transverse fields are $g^* \in \{0.48, 0.45, 0.435, 0.43\}$ such that the minimum of the spectral gap along the adiabatic path occurs close to $\lambda = 0.5$. (b) The spectral gap and (c) ground-state entanglement entropy for the $N = 23$ qubit Hamiltonian with and without the gauge potential. In this example $\tilde{A}^{(\chi)}(\lambda)$ is calculated using the method presented in Sec. II B with a bond dimension $\chi = 4$. The entanglement entropy corresponds to that of the MPS ground state found using standard density-matrix renormalization group (DMRG) algorithms [32], in particular we calculate the mean von-Neumann entropy across partitions to the right of sites $(N-1)/2$ and $(N+1)/2$ of the chain.

U^{Trotter}, we divide the total adiabatic evolution time T into $R = 8$ equal time chunks labelled by $r = 1, 2, \ldots, R$. We then construct a second-order Trotter approximation of $U_r^{\text{Trotter}} \approx \exp(-\mathrm{i}T/R\mathcal{H}(\lambda(t_r)))$ keeping $\mathcal{H}$ fixed during each chunk, where t_r is the time corresponding the the midpoint of the r^{th} chunk. The full Trotterized adiabatic evolution is then given by the time-ordered product $U^{\text{Trotter}} = \prod_{r=1}^{8} U_r^{\text{Trotter}}$.

In order to quantify the errors due to imperfect adiabatic evolution, we compute the fidelity between the state prepared by each circuit and the corresponding exact Hamiltonian ground states, in addition to errors in the energies of these states. These values are defined in terms of the exact ground state of the Hamiltonian H_s at slice s denoted $|\psi_s\rangle$ as well as those of the initial and final Hamiltonians $|\psi_i\rangle$ and $|\psi_f\rangle$, respectively. We calculate these ground states numerically exactly using standard DMRG methods. After applying the adiabatic evolution circuits to the initial state, we are left with $|\phi_s\rangle = U_s |\psi_i\rangle$ where U_s is the circuit preparing the state at slice s. The target fidelity is defined as

$$\mathcal{F}_s^{\text{targ}} = |\langle\phi_s|\psi_f\rangle|^2 \tag{10}$$

and the target energy error is given by the relative error

$$\mathcal{E}_s^{\text{targ}} = \left(\langle\phi_s| H_f |\phi_s\rangle - \langle\psi_s| H_f |\psi_s\rangle\right) / \langle\psi_s| H_f |\psi_s\rangle . \tag{11}$$

We also consider the instantaneous energy error defined by

$$\mathcal{E}_s^{\text{inst}} = \left(\langle\phi_s| H_s |\phi_s\rangle - \langle\psi_s| H_s |\psi_s\rangle\right) / \langle\psi_s| H_s |\psi_s\rangle , \tag{12}$$

where we note that $\mathcal{E}_s^{\text{targ}}$ and $\mathcal{E}_s^{\text{inst}}$ are equivalent at the final time slice.

The results are presented in Fig. 6. For the parameters chosen, we observe that classically optimized counterdiabatic circuits outperform the standard adiabatic Trotter circuits. For both the target fidelity and energy error, the value obtained is improved using a larger bond dimension for the variationally optimized MPO gauge potential. Furthermore, for $N = 7$ qubits we observe that classically optimized variational circuits outperform the ideal nested commutator dynamics for all orders $l \leq 6$. Across all system sizes we observe that classically optimized counterdiabatic circuits outperform the best Trotter result by a factor of 5 for the target fidelities and a factor of 3 for the ground state energy errors.

IV. DISCUSSION

In this article, we numerically demonstrate that adiabatic evolution with counterdiabatic driving for specific, one-dimensional quantum many-body systems can be accurately represented by appending shallow one-dimensional quantum circuits that are optimized using standard tensor-network techniques. The approach can be readily applied to two-dimensional quantum many-body systems by making use of the corresponding two-dimensional tensor-network algorithms [15–17]. More specifically, shallow two-dimensional quantum circuits can be expressed in terms of so-called projected entangled pair states [33] for which powerful optimization methods are known, e.g. [33–37].

An interesting question is whether the quantum circuit optimization procedures can also be used to adiabatically solve combinatorial optimization problems, which have historically always been an important application for adiabatic quantum computing [1–4]. For one-dimensional classical systems, it makes sense to use the same approach as for the quantum systems and optimize shallow

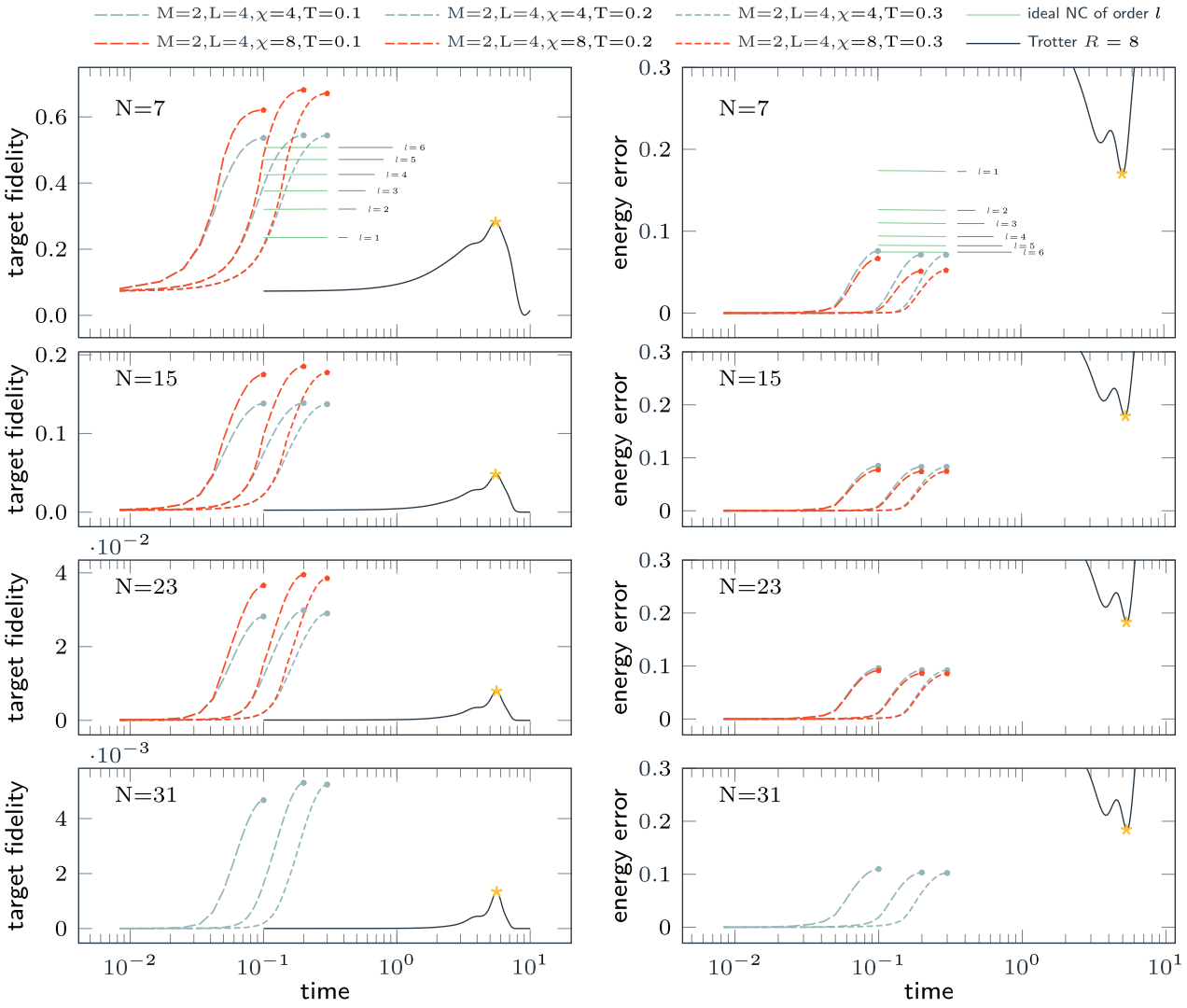

FIG. 6. The target fidelity of Eq. (10) (left column) and energy error of Eqs. (11) and (12) (right column) achieved using either a second-order Trotterization of the standard adiabatic path or classically optimized counterdiabatic circuits for the antiferromagnetic quantum Ising gap traversal problem defined in Sec. III B. For each system size N, all circuits considered contain the same number of two-qubit gates $R(N-1)$ where $R = M \times L = 8$. The solid black line indicates the target fidelity and energy error achieved by the Trotter circuit at the *end* of a standard adiabatic sweep, i.e. at $\lambda(T) = 1$, for total evolution times T up to a maximum $T = 10$. The best values achieved by the Trotter circuits are indicated by a star symbol. The dashed blue and red lines indicate the target fidelity or instantaneous energy error achieved during the adiabatic evolution using the classically optimized counterdiabatic circuits where the counterdiabatic gauge potentials are calculated as MPOs of bond dimension χ. The maximum target fidelities and minimum energy errors are achieved at the end of the adiabatic path and are indicated by blue circles (red pentagons) for $\chi = 4$ ($\chi = 8$). Additionally, the solid green lines indicate the target fidelities and energy errors achieved by ideal adiabatic evolution aided by an order l nested commutator (NC) gauge potential.

one-dimensional quantum circuits to realize the adiabatic protocol. Figure 7 shows results for 10 random instances of classical nearest-neighbour Ising chains. We see that, similar to the quantum counterpart, the methods work and the classically optimized circuits outperform Trotter circuits. We emphasize, however, that one-dimensional classical spin systems can be efficiently solved using classical computers.

For the more interesting, hard classical problems with nonlocal interactions, including quadratic unconstrained binary optimization [38, 39], we propose to use a variational circuit architecture consisting of three parts. The first part is a circuit structure that can be efficiently classically worked with, for instance a shallow brickwork circuit or a tensor-network-inspired quantum circuit as considered, e.g., in [40–42]. The second part is composed of commuting many-qubit gates, e.g. one layer of the quantum approximate optimization algorithm (QAOA) [6] where, however, each gate contributes an independent variational parameter as in multi-angle QAOA [43]. The

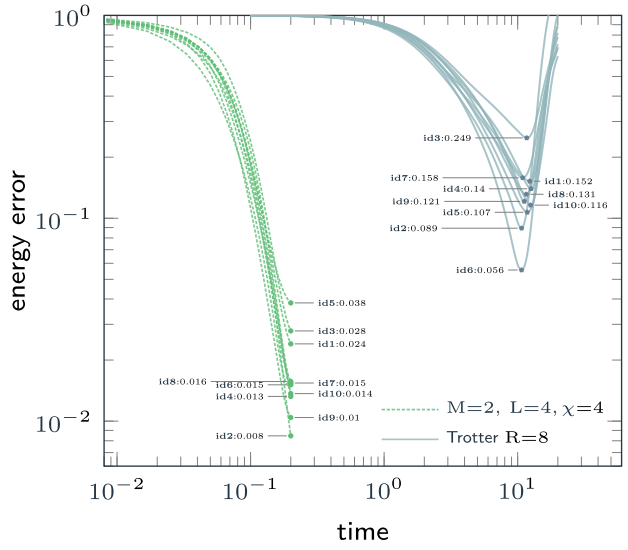

FIG. 7. Energy error achieved by circuits of $R = M \times L = 8$ layers for random instances, $\mathbf{id} \in \{1, 2, \ldots, 10\}$, of the nearest-neighbour Ising Hamiltonian Eq. (5) with $N = 8$ qubits. For the initial Hamiltonian we choose $g_k = 0.5\ \forall k$ and $J_k = h_k = 0\ \forall k$. For the final Hamiltonian, couplings J_k and local fields h_k are chosen randomly from the sets $J_k \in \pm\{0.2, 0.4, 0.6, 0.8, 1.0\}$, $h_k \in \pm\{0.0, 0.2, 0.4, 0.6, 0.8\}$ and $g_k = 0\ \forall k$. For each of the 10 instances, the target energy error Eq. (11) of the classically optimized counterdiabatic circuits along the linear adiabatic path, $\lambda(t) = t/T$ with $T = 0.2$, from $\lambda = 0$ to $\lambda = 1$ is indicated by the dashed green lines. Additionally, for each instance we plot the energy error achieved at the *end* of the adiabatic path, i.e. at $\lambda = 1$ only, by a second-order Trotter circuit following the standard linear adiabatic path for a range of total times T, up to a maximum total time $T = 20$. In all cases, the minimum energy achieved is indicated by a pentagon (circle) for Trotter (classically optimized counterdiabatic) and is labelled with its instance number alongside the numerical value of the error.

third part consists of one layer of arbitrary single-qubit gates. A quantum circuit consisting of these three parts can be efficiently classically optimized using tensor network algorithms for so-called weighted graph states [44–48]. We present an example circuit architecture of this type in Fig. 8.

Appendix A: Adiabatic gauge potential

In this Appendix, we provide a brief derivation of the adiabatic gauge potential and some of its properties; see [21] for a more comprehensive presentation.

We consider a general Hamiltonian $\mathcal{H}(\lambda)$ depending on a scalar λ, which can, e.g., be of the particular form $\mathcal{H}(\lambda) = (1-\lambda)H_i + \lambda H_f$ used in Fig. 1 (a). We define the unitary $U(\lambda)$ that diagonalizes $\mathcal{H}(\lambda)$,

$$U^\dagger(\lambda)\mathcal{H}(\lambda)U(\lambda) = \tilde{\mathcal{H}}(\lambda), \tag{A1}$$

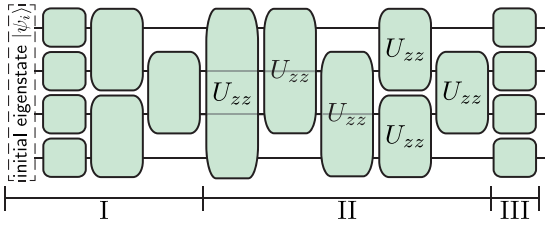

FIG. 8. Part I is a brickwork circuit of $L = 1$ layer. The component inside the dashed box needs to be included only in the first chunk optimization of Fig. 1. Part II consists of commuting two-qubit gates acting on all possible pairs of qubits and part III contains generic single-qubit gates. The gate parameterization is defined in Fig. 2.

where $\tilde{\mathcal{H}}(\lambda)$ is diagonal and contains the eigenvalues of $\mathcal{H}(\lambda)$. In other words, the kth column of $U(\lambda)$ contains the eigenvector $|k(\lambda)\rangle$ of $\mathcal{H}(\lambda)$ to eigenvalue $E_k(\lambda)$, which is the kth entry on the diagonal of $\tilde{\mathcal{H}}(\lambda)$. This is equivalent to

$$\begin{aligned} \mathcal{H}(\lambda) &= U(\lambda)\tilde{\mathcal{H}}(\lambda)U^\dagger(\lambda) && \text{(A2)} \\ &= \sum_k E_k(\lambda)|k(\lambda)\rangle\langle k(\lambda)| && \text{(A3)} \end{aligned}$$

where $(\cdot)^\dagger$ is the adjoint of $(\cdot)$. In the adiabatic protocol $\lambda = \lambda(t)$ and so we refer to the eigenstates $|k(\lambda)\rangle$ as the instantaneous eigenstates. For an arbitrary operator O we define $\tilde{O} = U^\dagger(\lambda)OU(\lambda)$ its representation in the instantaneous eigenbasis. Similarly for an arbitrary state $|\psi\rangle$ we define $|\tilde{\psi}\rangle = U^\dagger(\lambda)|\psi\rangle$.

We want to write the time-dependent Schrödinger equation in the instantaneous eigenbasis. To that end, we consider the time-derivative of the components of $|\psi\rangle$ in the instantanous eigenbasis, i.e. $\partial_t|\tilde{\psi}\rangle$, for which we obtain

$$\begin{aligned} \mathrm{i}\partial_t|\tilde{\psi}\rangle &= \mathrm{i}\partial_t\left(U^\dagger|\psi\rangle\right) && \text{(A4)} \\ &= \mathrm{i}\left(\partial_t U^\dagger\right)|\psi\rangle + \mathrm{i}U^\dagger\left(\partial_t|\psi\rangle\right) && \text{(A5)} \\ &= \mathrm{i}\left(\partial_t\lambda\right)\left(\partial_\lambda U^\dagger\right)UU^\dagger|\psi\rangle + U^\dagger\mathcal{H}|\psi\rangle && \text{(A6)} \\ &= \mathrm{i}\dot{\lambda}\left(\partial_\lambda U^\dagger\right)U|\tilde{\psi}\rangle + U^\dagger\mathcal{H}UU^\dagger|\psi\rangle && \text{(A7)} \\ &= -\dot{\lambda}\tilde{A}|\tilde{\psi}\rangle + \tilde{\mathcal{H}}|\tilde{\psi}\rangle. && \text{(A8)} \end{aligned}$$

Here we have used $\mathrm{i}\partial_t|\psi\rangle = \mathcal{H}|\psi\rangle$. We have defined $\partial_t\lambda = \dot{\lambda}$ and the gauge potential

$$\tilde{A} = -\mathrm{i}\left(\partial_\lambda U^\dagger\right)U \tag{A9}$$

in the instantaneous eigenbasis, which reads

$$A = -\mathrm{i}U\left(\partial_\lambda U^\dagger\right) \tag{A10}$$

in the standard eigenbasis.

Equation (A8) implies that, in the instantaneous eigenbasis the evolution happens according to $\tilde{\mathcal{H}} - \dot{\lambda}\tilde{A}$. Therefore, if the initial state is an eigenstate of $\mathcal{H}$, then $\tilde{A}$

causes the state to deviate from the instantaneous eigenbasis during the evolution. We counteract this deviation by using $\mathcal{H} + \dot{\lambda}A$ instead of just $\mathcal{H}$ in the Schrödinger equation. Then, assuming the exact A is used, an initial eigenstate of $\mathcal{H}$ propagates as an exact instantaneous eigenstate during the entire evolution.

The adiabatic gauge potential is Hermitian,

$$\begin{aligned} A^\dagger &= \left(-\mathrm{i}U\left(\partial_\lambda U^\dagger\right)\right)^\dagger && \text{(A11)}\\ &= \mathrm{i}\left(\partial_\lambda U^\dagger\right)^\dagger U^\dagger && \text{(A12)}\\ &= \mathrm{i}\left(\partial_\lambda U\right)U^\dagger && \text{(A13)}\\ &= \mathrm{i}\partial_\lambda\left(UU^\dagger\right) - \mathrm{i}U\left(\partial_\lambda U^\dagger\right) && \text{(A14)}\\ &= -\mathrm{i}U\left(\partial_\lambda U^\dagger\right) && \text{(A15)}\\ &= A, && \text{(A16)} \end{aligned}$$

where we have used $\partial_\lambda(UU^\dagger) = \partial_\lambda \mathbb{1} = 0$ and $\mathbb{1}$ is the identity operator. Note that, for a real-valued Hamiltonian $\mathcal{H}$, U can be chosen to be a real-valued orthogonal matrix and then A contains only imaginary numbers.

In terms of the instantaneous eigenstates $|k\rangle$ and eigenenergies E_k, A in Eq. (A10) takes on the form

$$\begin{aligned} A &= -\mathrm{i}\sum_k |k\rangle\left(\partial_\lambda\langle k|\right) && \text{(A17)}\\ &= -\mathrm{i}\sum_k\sum_{l\neq k}\frac{\langle k|\left(\partial_\lambda\mathcal{H}\right)|l\rangle}{E_k - E_l}|k\rangle\langle l|, && \text{(A18)} \end{aligned}$$

where we have used $(\partial_\lambda\mathcal{H})^\dagger = \partial_\lambda\mathcal{H}$ and

$$\partial_\lambda|k\rangle = \sum_{l\neq k}\frac{\langle l|\left(\partial_\lambda\mathcal{H}\right)|k\rangle}{E_k - E_l}|l\rangle. \quad \text{(A19)}$$

This follows, e.g., from differentiating the time-independent Schrödinger equation $\mathcal{H}|k\rangle = E_k|k\rangle$ with respect to λ,

$$\left(\partial_\lambda\mathcal{H}\right)|k\rangle + \mathcal{H}\left(\partial_\lambda|k\rangle\right) = \left(\partial_\lambda E_k\right)|k\rangle + E_k\left(\partial_\lambda|k\rangle\right), \quad \text{(A20)}$$

which, multiplied from the left by $\langle l|$, leads to

$$\langle l|\left(\partial_\lambda|k\rangle\right) = \frac{\langle l|\left(\partial_\lambda\mathcal{H}\right)|k\rangle}{E_k - E_l} \quad \text{(A21)}$$

for all $l \neq k$. For $l = k$, we remember that A is Hermitian and for a real-valued Hamiltonian $\mathcal{H}$ we can choose A to contain only imaginary numbers, so that

$$\begin{aligned} \langle k|A|k\rangle &= \langle k|A^\dagger|k\rangle && \text{(A22)}\\ &= \left(\langle k|A|k\rangle\right)^* && \text{(A23)}\\ &= 0 && \text{(A24)} \end{aligned}$$

where $(\cdot)^*$ is the complex conjugate of $(\cdot)$.

Appendix B: Variational gauge potential

In this Appendix, we present a concise derivation of the cost function that we minimize in the main text using a variational ansatz for the adiabatic gauge potential; see [21] for further details.

We define the operators

$$\begin{aligned} G &= \left(\partial_\lambda\mathcal{H}\right) + \mathrm{i}[A,\mathcal{H}], && \text{(B1)}\\ M &= \sum_k\left(\partial_\lambda E_k\right)|k\rangle\langle k|, && \text{(B2)} \end{aligned}$$

where $[O_1, O_2]$ is the commutator of O_1 and O_2. The operators G and M are equivalent to each other, i.e. $G = M$, for the exact gauge potential A. This can be seen by differentiating $\mathcal{H}$ with respect to λ,

$$\begin{aligned} \partial_\lambda\mathcal{H} &= \partial_\lambda\left(U\tilde{\mathcal{H}}U^\dagger\right) && \text{(B3)}\\ &= \left(\partial_\lambda U\right)\tilde{\mathcal{H}}U^\dagger + U\left(\partial_\lambda\tilde{\mathcal{H}}\right)U^\dagger + \\ &\quad U\tilde{\mathcal{H}}\left(\partial_\lambda U^\dagger\right) && \text{(B4)}\\ &= \left(\partial_\lambda U\right)U^\dagger\mathcal{H} + \sum_k\left(\partial_\lambda E_k\right)|k\rangle\langle k| + \\ &\quad \mathcal{H}U\left(\partial_\lambda U^\dagger\right) && \text{(B5)}\\ &= -\mathrm{i}A\mathcal{H} + \sum_k\left(\partial_\lambda E_k\right)|k\rangle\langle k| + \mathrm{i}\mathcal{H}A && \text{(B6)}\\ &= -\mathrm{i}[A,\mathcal{H}] + \sum_k\left(\partial_\lambda E_k\right)|k\rangle\langle k|, && \text{(B7)} \end{aligned}$$

where we have used Eqs. (A1), (A2), (A3), (A10) and (A13). Note that, because M commutes with $\mathcal{H}$, G commutes with $\mathcal{H}$ for the exact gauge potential A.

Following [21], we define as the goal of the variational procedure the optimization of a variational ansatz $\tilde{A}$ for A in $G(A)$, see Eq. (B1), to minimize the Frobenius distance

$$\begin{aligned} \epsilon(\tilde{A}) &= \mathrm{tr}\left[\left(G(\tilde{A}) - M\right)^\dagger\left(G(\tilde{A}) - M\right)\right] && \text{(B8)}\\ &= \mathrm{tr}\left[G^\dagger(\tilde{A})G(\tilde{A})\right] - 2\,\mathrm{Re}\{\mathrm{tr}\left[G^\dagger(\tilde{A})M\right]\} + \\ &\quad \mathrm{tr}\left[M^\dagger M\right] && \text{(B9)} \end{aligned}$$

where $\mathrm{tr}[\cdot]$ is the trace of $[\cdot]$ and $\mathrm{Re}\{\cdot\}$ is the real part of $\{\cdot\}$. We see that

$$\begin{aligned} \mathrm{tr}\left[G^\dagger M\right] &= \mathrm{tr}\left[\left(\left(\partial_\lambda\mathcal{H}\right) + \mathrm{i}[\tilde{A},\mathcal{H}]\right)^\dagger M\right] && \text{(B10)}\\ &= \mathrm{tr}\left[\left(\partial_\lambda\mathcal{H}\right)^\dagger M\right] - \mathrm{itr}\left[\mathcal{H}\tilde{A}^\dagger M\right] + \\ &\quad \mathrm{itr}\left[\tilde{A}^\dagger\mathcal{H}M\right] && \text{(B11)}\\ &= \mathrm{tr}\left[\left(\partial_\lambda\mathcal{H}\right)^\dagger M\right] - \mathrm{itr}\left[\tilde{A}^\dagger M\mathcal{H}\right] + \\ &\quad \mathrm{itr}\left[\tilde{A}^\dagger M\mathcal{H}\right] && \text{(B12)}\\ &= \mathrm{tr}\left[\left(\partial_\lambda\mathcal{H}\right)^\dagger M\right] \\ &= \mathrm{tr}\left[M^\dagger M\right], && \text{(B13)} \end{aligned}$$

where we have used the cyclic property of the trace and that M commutes with $\mathcal{H}$. Also, we have inserted

Eq. (B7) and evaluated the resulting expression. Therefore the Frobenius distance in Eq. (B8) is

$$\epsilon(\tilde{A}) \;=\; \mathrm{tr}[G^\dagger(\tilde{A})G(\tilde{A})] - \mathrm{tr}[M^\dagger M]. \qquad \text{(B14)}$$

Because M does not depend on $\tilde{A}$, we minimize the Frobenius distance in Eq. (B8) variationally via $\tilde{A}$ by minimizing the cost function

$$\mathcal{C}(\tilde{A}) = \mathrm{tr}\left[G^\dagger(\tilde{A})G(\tilde{A})\right]. \qquad \text{(B15)}$$

This cost function can be alternatively derived starting from the system of linear equations

$$\left[\mathcal{H}, \tilde{A}\right] = -\mathrm{i}\,(\partial_\lambda \mathcal{H}) \qquad \text{(B16)}$$

and solving them for a variational $\tilde{A}$ by minimizing the Frobenius distance between the left-hand and right-hand side of Eq. (B16). Since tensor network algorithms for linear equations exist [25, 26], we use Eq. (B16) as the starting point for the variational MPO optimization in the main text.

[1] T. Kadowaki and H. Nishimori, Quantum annealing in the transverse Ising model, Phys. Rev. E **58**, 5355 (1998).
[2] E. Farhi, J. Goldstone, S. Gutmann, and M. Sipser, Quantum Computation by Adiabatic Evolution (2000), arXiv:quant-ph/0001106 [quant-ph].
[3] T. Albash and D. A. Lidar, Adiabatic quantum computation, Rev. Mod. Phys. **90**, 015002 (2018).
[4] P. Hauke, H. G. Katzgraber, W. Lechner, H. Nishimori, and W. D. Oliver, Perspectives of quantum annealing: methods and implementations, Rep. Prog. Phys. **83**, 054401 (2020).
[5] M. W. Johnson, M. H. S. Amin, S. Gildert, T. Lanting, F. Hamze, N. Dickson, R. Harris, A. J. Berkley, J. Johansson, P. Bunyk, E. M. Chapple, C. Enderud, J. P. Hilton, K. Karimi, E. Ladizinsky, N. Ladizinsky, T. Oh, I. Perminov, C. Rich, M. C. Thom, E. Tolkacheva, C. J. S. Truncik, S. Uchaikin, J. Wang, B. Wilson, and G. Rose, Quantum annealing with manufactured spins, Nature **473**, 194 (2011).
[6] E. Farhi, J. Goldstone, and S. Gutmann, A Quantum Approximate Optimization Algorithm (2014), arXiv:1411.4028 [quant-ph].
[7] C. Zener, Non-adiabatic crossing of energy levels, Proc. R. Soc. Lond. A **137**, 696 (1932).
[8] S. Lloyd, Universal Quantum Simulators, Science **273**, 1073 (1996).
[9] M. Demirplak and S. A. Rice, Adiabatic Population Transfer with Control Fields, J. Phys. Chem. A **107**, 9937 (2003).
[10] M. Demirplak and S. A. Rice, Assisted Adiabatic Passage Revisited, J. Phys. Chem. B **109**, 6838 (2005).
[11] M. V. Berry, Transitionless quantum driving, J. Phys. A: Math. Theor. **42**, 365303 (2009).
[12] M. Benedetti, E. Lloyd, S. Sack, and M. Fiorentini, Parameterized quantum circuits as machine learning models, Quantum Sci. Technol. **4**, 043001 (2019).
[13] M. Cerezo, A. Arrasmith, R. Babbush, S. C. Benjamin, S. Endo, K. Fujii, J. R. McClean, K. Mitarai, X. Yuan, L. Cincio, and P. J. Coles, Variational quantum algorithms, Nat. Rev. Phys. **3**, 625 (2021).
[14] K. Bharti, A. Cervera-Lierta, T. H. Kyaw, T. Haug, S. Alperin-Lea, A. Anand, M. Degroote, H. Heimonen, J. S. Kottmann, T. Menke, W.-K. Mok, S. Sim, L.-C. Kwek, and A. Aspuru-Guzik, Noisy intermediate-scale quantum algorithms, Rev. Mod. Phys. **94**, 015004 (2022).
[15] V. M. F. Verstraete and J. I. Cirac, Matrix product states, projected entangled pair states, and variational renormalization group methods for quantum spin systems, Adv. Phys. **57**, 143 (2008).
[16] R. Orús, A practical introduction to tensor networks: Matrix product states and projected entangled pair states, Ann. Phys. **349**, 117 (2014).
[17] M. C. Bañuls, Tensor Network Algorithms: A Route Map, Annu. Rev. Condens. Matter Phys. **14**, 173 (2023).
[18] R. Mansuroglu, T. Eckstein, L. Nützel, S. A. Wilkinson, and M. J. Hartmann, Variational Hamiltonian simulation for translational invariant systems via classical preprocessing, Quantum Sci. Technol. **8**, 025006 (2023).
[19] M. S. J. Tepaske, D. Hahn, and D. J. Luitz, Optimal compression of quantum many-body time evolution operators into brickwall circuits, SciPost Phys. **14**, 073 (2023).
[20] C. Mc Keever and M. Lubasch, Classically optimized Hamiltonian simulation, Phys. Rev. Res. **5**, 023146 (2023).
[21] M. Kolodrubetz, D. Sels, P. Mehta, and A. Polkovnikov, Geometry and non-adiabatic response in quantum and classical systems, Phys. Rep. **697**, 1 (2017).
[22] F. Verstraete, J. J. García-Ripoll, and J. I. Cirac, Matrix Product Density Operators: Simulation of Finite-Temperature and Dissipative Systems, Phys. Rev. Lett. **93**, 207204 (2004).
[23] M. Zwolak and G. Vidal, Mixed-State Dynamics in One-Dimensional Quantum Lattice Systems: A Time-Dependent Superoperator Renormalization Algorithm, Phys. Rev. Lett. **93**, 207205 (2004).
[24] P. W. Claeys, M. Pandey, D. Sels, and A. Polkovnikov, Floquet-Engineering Counterdiabatic Protocols in Quantum Many-Body Systems, Phys. Rev. Lett. **123**, 090602 (2019).
[25] I. V. Oseledets and S. V. Dolgov, Solution of Linear Systems and Matrix Inversion in the TT-Format, SIAM J. Sci. Comput. **34**, A2718 (2012).
[26] M. Lubasch, P. Moinier, and D. Jaksch, Multigrid renormalization, J. Comp. Phys. **372**, 587 (2018).
[27] M. P. Zaletel, R. S. K. Mong, C. Karrasch, J. E. Moore, and F. Pollmann, Time-evolving a matrix product state with long-ranged interactions, Phys. Rev. B **91**, 165112 (2015).
[28] M. V. Damme, J. Haegeman, I. McCulloch, and L. Vanderstraeten, Efficient higher-order matrix product operators for time evolution (2023), arXiv:2302.14181 [cond-mat.str-el].

[29] J. Feist and contributors, Quantumalgebra.jl (2021).

[30] M. Fishman, S. R. White, and E. M. Stoudenmire, The ITensor Software Library for Tensor Network Calculations, SciPost Phys. Codebases , 4 (2022).

[31] M. Fishman, S. R. White, and E. M. Stoudenmire, Codebase release 0.3 for ITensor, SciPost Phys. Codebases , 4 (2022).

[32] U. Schollwöck, The density-matrix renormalization group, Rev. Mod. Phys. **77**, 259 (2005).

[33] F. Verstraete and J. I. Cirac, Renormalization algorithms for quantum many-body systems in two and higher dimensions (2004), arXiv:cond-mat/0407066 [cond-mat.str-el].

[34] M. Lubasch, J. I. Cirac, and M.-C. Bañuls, Unifying projected entangled pair state contractions, New J. Phys. **16**, 033014 (2014).

[35] M. Lubasch, J. I. Cirac, and M.-C. Bañuls, Algorithms for finite projected entangled pair states, Phys. Rev. B **90**, 064425 (2014).

[36] P. Czarnik, J. Dziarmaga, and P. Corboz, Time evolution of an infinite projected entangled pair state: An efficient algorithm, Phys. Rev. B **99**, 035115 (2019).

[37] C. Mc Keever and M. H. Szymańska, Stable iPEPO Tensor-Network Algorithm for Dynamics of Two-Dimensional Open Quantum Lattice Models, Phys. Rev. X **11**, 021035 (2021).

[38] A. Lucas, Ising formulations of many NP problems, Front. Phys. **2**, 10.3389/fphy.2014.00005 (2014).

[39] F. Glover, G. Kochenberger, R. Hennig, and Y. Du, Quantum bridge analytics I: a tutorial on formulating and using QUBO models, Ann. Oper. Res. **314**, 141 (2022).

[40] R. Haghshenas, J. Gray, A. C. Potter, and G. K.-L. Chan, Variational Power of Quantum Circuit Tensor Networks, Phys. Rev. X **12**, 011047 (2022).

[41] E. Cervero Martín, K. Plekhanov, and M. Lubasch, Barren plateaus in quantum tensor network optimization, Quantum **7**, 974 (2023).

[42] R. Haghshenas, E. Chertkov, M. DeCross, T. M. Gatterman, J. A. Gerber, K. Gilmore, D. Gresh, N. Hewitt, C. V. Horst, M. Matheny, T. Mengle, B. Neyenhuis, D. Hayes, and M. Foss-Feig, Probing critical states of matter on a digital quantum computer (2023), arXiv:2305.01650 [quant-ph].

[43] R. Herrman, P. C. Lotshaw, J. Ostrowski, T. S. Humble, and G. Siopsis, Multi-angle quantum approximate optimization algorithm, Sci. Rep. **12**, 6781 (2022).

[44] S. Anders, M. B. Plenio, W. Dür, F. Verstraete, and H.-J. Briegel, Ground-State Approximation for Strongly Interacting Spin Systems in Arbitrary Spatial Dimension, Phys. Rev. Lett. **97**, 107206 (2006).

[45] S. Anders, H. J. Briegel, and W. Dür, A variational method based on weighted graph states, New J. Phys. **9**, 361 (2007).

[46] L. Hartmann, J. Calsamiglia, W. Dür, and H. J. Briegel, Weighted graph states and applications to spin chains, lattices and gases, J. Phys. B: At., Mol. Opt. Phys. **40**, S1 (2007).

[47] R. Hübener, C. Kruszynska, L. Hartmann, W. Dür, F. Verstraete, J. Eisert, and M. B. Plenio, Renormalization algorithm with graph enhancement, Phys. Rev. A **79**, 022317 (2009).

[48] R. Hübener, C. Kruszynska, L. Hartmann, W. Dür, M. B. Plenio, and J. Eisert, Tensor network methods with graph enhancement, Phys. Rev. B **84**, 125103 (2011).